MIT Open Access Articles

Numerical Simulation of Stent Angioplasty with Predilation: An Investigation into Lesion Constitutive Representation and Calcification Influence

Massachusetts Institute of Technology

Numerical Simulation of Stent Angioplasty with Predilation: an Investigation into Lesion Constitutive Representation and Calcification Influence

Conway, C.[1,2,*], McGarry, J.P.[1] Edelman, E.R.[2,3] and McHugh, P.E.[1]

[1]   Biomechanics Research Centre (BMEC), Biomedical Engineering, College of

Engineering and Informatics, National University of Ireland Galway, Ireland.

[2]   Institute for Medical Engineering and Science (IMES), Massachusetts Institute of

Technology, Cambridge, MA, USA.

[3]   Cardiovascular Division, Brigham and Women's Hospital, Harvard Medical School,

Boston, MA, USA.

* Corresponding author contact information:

Email: cconway@mit.edu

Phone: +1-617-258-8893

Abstract

It is acceptable clinical practice to predilate a severely occluded vessel to allow better positioning of endovascular stents, and while the impact of this intervention has been examined for aggregate response in animals there has been no means to examine whether there are specific vessels that might benefit. Finite element methods offer the singular ability to explore the mechanical response of arteries with specific pathologic alterations in mechanics to stenting and predilation. We examined varying representations of atherosclerotic tissue including homogeneous and heterogeneous dispersion of calcified particles, and elastic, pseudo-elastic, and elastic-plastic constitutive representations of bulk atherosclerotic tissue. The constitutive representations of the bulk atherosclerotic tissue were derived from experimental test data and highlight the importance of accounting for testing mode of loading. The impact of arterial predilation is presented and, in particular, its effect on intimal predicted damage, atherosclerotic tissue von Mises and maximum principal stresses, and luminal deformation was dependent on the type of constitutive representation of diseased tissue, particularly in the presence of calcifications.

Key words: Stent, Atherosclerosis, Predilation Angioplasty, Finite Element Analysis, Pseudo-Elasticity, Calcification

Introduction

Standard stent implantation mandates balloon predilation to open and prepare blocked vessels to facilitate stent passage and positioning [1]. Predilation is an accepted part of the angioplasty protocol, especially when there is observable calcification. However, the effects of predilation and accompanying additional mechanical vessel trauma are not fully understood.

Clinical trials have examined population responses to the need for predilation or success of direct angioplasty without such intervention but there has not been a systematic investigation as to how the artery and in particular different lesion types respond to predilation. Such an analysis is best performed using computational methods as only such an analysis can control arterial characteristics at the outset. Studies in normal animals and clinical trials across a wide population range have been performed but there is no insight as to whether specific lesions and particular lesion elements would more naturally benefit or be harmed by such intervention [2,3]. The heterogeneity of the six-decade old human lesion and the variability in the animal model preclude these platforms. Models of angioplasty have been performed but rarely if at all by varying the lesion and artery boundary conditions.

In silico representations of lesions are ideal for such analysis and indeed predictive finite element simulations are used ubiquitously to describe the clinical practice of stenting. Finite element analysis has offered precise quantification of vessel mechanical state and insight into direct stenting angioplasty [4–13]. However, these simulations have not taken into account predilation. This work provides insight into the effect of predilation on the vessel structural state and furthermore quantifies the effect of diseased tissue elements.

3

Moreover, most have modelled stent angioplasty against a backdrop of almost exclusively hyperelastic constitutive representations of atherosclerotic tissue [5,14]. While, much of the vessel is elastic and indeed stents were invented to mediate against elastic recoil in arteries the human lesion is necessarily replete with sclerotic, calcific and non-elastic elements. In fact, the calcific vascular deposits often dictate the need for predilation. What we do not know and cannot tell except through modelling is to what extent such elements influence procedural efficiency and efficacy. It is for this reason that we include a tissue damage model, in particular the Mullins effect model [15], which is commonly utilised for the representation of damage induced stress softening in soft tissue [5,15–21] and in combination with differential order Odgen [22] models enabled precise determination of lesion characteristic. Also implemented is an elastic-plastic representation of atherosclerotic tissue, and model both homogeneous, and heterogeneous tissue with dispersed calcified particles.

In short, we use computational modelling to determine the domains in which arterial tissue representations are valid predictors of the effects and response of different aspects of the stent implantation procedure.

Materials & Methods

Geometry & Meshes

The stent angioplasty population-specific computational test-bed with a 50% stenosed three layer arterial model previously presented in [4,5] was used as a basis for this work. A two-phase expansion simulation strategy was employed: the artery was first expanded to simulate balloon-only expansion; then allowed to recoil and expand again, with a stent deployed on the second expansion. The effects of the inclusion of the Mullins effect (pseudo-elastic) and elastic-plastic representations within the atherosclerotic tissue material model on the arterial and stent deployment mechanics were then assessed and discussed. Finally, the presence of calcified particles was also assessed for all diseased population types considered.

The test-bed utilised the commercially available Abaqus/Explicit solver (v6.13-5 DS SIMULIA, USA). For the present study, a straight coronary artery with a 50% stenotic lesion (measured by cross-sectional area) was selected (Figure 1). Homogeneous and heterogeneous representations of the stenotic lesion were considered, with the geometry of the heterogeneous tissue including dispersed calcified particles [5]. 630 calcified particles were randomly distributed in the atherosclerotic bulk (Figure 1) and this represented 0.5% of the total atherosclerotic tissue volume. The approximate size of a particle was 0.0002 mm^3 as determined from histological observations from literature [23]. It is important to note that while the geometry used in this study represents a population of coronary vasculature, there are implications for the representation of diseased arterial tissue in simulations of peripheral stenting procedures as well.

A generic stent geometry was used in this study that is representative of the Cypher closed-cell stent, meshed with 30,000 3D reduced integration eight-noded hexahedral elements [4,5]. To achieve the two-phase expansion, a cylindrically expandable stiff tube, meshed with 6580 four-noded reduced integration shell elements, was included. The tube simplifies the simulation of balloon expansion, initially without, and subsequently with, the stent. The appropriateness of using such a tube to simplify stent angioplasty simulations has been verified by Grogan *et al.* [24].

Constitutive Models

The constitutive behaviour of the healthy arterial wall and surrounding outer layer were extracted from the literature [4]. The responses of several types of diseased tissue in the vessel were considered and described by different mathematical representations including a first order Odgen [22] model (referred to as OgN1), a sixth order Ogden model (OgN6) and a second order hyperelastic polynomial (P2).

The choice of mathematical fit was motivated by the different experimental testing mode in each case. The OgN1 model tissue was fit to compressive test data of atherosclerotic tissue [17]. The OgN1 fit is soft in compression and tension. The P2 model tissue was fit to tensile test data of atherosclerotic tissue [25]. The P2 model fit is stiff in compression and tension. The OgN6 model compressive response was fit compressive test data and the tensile response was fit to tensile test data, resulting in a "hybrid" fit that is soft in compression and stiff in tension.

Stress softening upon unloading of fibrous tissue, including arterial tissue [20] and atherosclerotic plaque [17], exposed to cyclic loading is referred to as the Mullins effect. This

6

phenomenon, attributed to damage accumulation, was developed here and applied to the diseased tissue states. The responses to cyclic strain controlled loading of the OgN1 and OgN6 models included the Mullins effect (Figure 2). Also included was the elastic-plastic combination of the P2 model and plasticity (see Figure 2 for monotonic response), as there is experimental evidence of permanent deformation possible with this tissue type [17].

The motivation for the choice of pseudo-damage model approach is based on the availability of test data for an appropriate fit. In the case of the OgN1 and OgN6 fits there is compressive cyclic data available [17], thus inclusion of the Mullins effect was possible. In the case of the P2 model the tensile data available was monotonic only [25] thus a plasticity approach was implemented to simulate the limited load-bearing capacity of the tissue when damaged. In particular, the plasticity approach simulated *almost* perfect plasticity, the yield stress applied was 0.4 MPa and linear isotropic hardening was implemented with a slight increase in yield stress at 1000% plastic strain (which is not reached in these simulations). This methodology was implemented due to numerical issues found when applying the hyperelastic P2 model with absolute perfect plasticity.

Calcific vascular domains were considered to be isotropic and linear elastic in terms of finite deformation strain and stress measures. They were represented by a high relative stiffness, as driven by experimental data of Ebenstein et al. [26], with a Young's Modulus of 1 GPa and a Poisson's ration of $\upsilon = 0.3$. The cylindrical tube used in the two-phase expansion simulations was modelled as elastic and has a Young's Modulus of 2000 GPa and a Poisson's Ratio of 0.3. All displacements of the tube are prescribed (described in *Boundary Conditions & Loading*) thus

this technique fundamentally treats the expanding tube as a very stiff moving surface, or as a simulated semi-compliant balloon. The stent constitutive material model used is fully described in [4,5].

Boundary Conditions & Loading

For the simulations, a uniform radial displacement was applied to all nodes of the cylindrical tube, while all other degrees of freedom were fully constrained (Figure 1F). This approach ensures that all vessel types modelled reach the same prescribed diameters at each stage of the simulated intervention.   In modelling predilation the tube was expanded first, with contact between the stent and tube switched "off", making the stent computationally "invisible". The tube was then deflated and re-inflated with contact between the stent and tube switched "on", making the stent computationally "visible", to simulate expansion. Finally, the tube was deflated leaving the stent in place as a scaffold for the artery.

The pseudo-elastic model of [15] is a discontinuous damage model where material damage on any loading path will only accumulate when the maximum strain energy experienced by the material for any previous loading cycle is exceeded. To allow for the possibility of plaque tissue damage due to both the predilation and the stent deployment, the maximum amplitude of the first loading cycle (stent "invisible") was 10% less than the second loading cycle (stent "visible") (Figure 1.A-E). The remainder of the boundary conditions were similar to those described in [4,5].

Analysis of Results

To investigate the influence of the predilation step in the simulations a comparison with direct stenting (no predilation step) was performed for three tissue representations: OgN1 and OgN6, with Mullins effect, and P2 with plasticity. The von Mises stress distribution in atherosclerotic lesion tissue was presented and compared at maximum stent inflation for each analysis type.

The results were then analysed in terms of lumen cross-sectional area (CSA) along the lesion length (Z-axis in Figure 1(A)). Clinically, the7 luminal area is quantified when intravascular imaging is performed post stent implantation. This predictive finite element measure provides insight into the variation of luminal area along the length of the lesion.

As an indicator of damage within the arterial vessel, the percent intimal tissue damage risk [4,5] was calculated. This measure represents the proportion of elements in the intimal layer of the artery wall with von Mises stress values exceeding experimentally reported ultimate tensile strength values for human intimal tissue, and specifically 394 MPa [4,27]. Finally, the atherosclerotic tissue maximum principal stress state for all populations considered were compared and assessed; to gain insight into the how these stress distributions are dependent on choice of elasticity model. Run times for these analyses were on the order of 600 CPU hours each on an Intel Xeon E2650 cluster.

Results

Predilation Influence on Atherosclerotic Tissue von Mises Stress Distribution

==When simulated, predilation is predicted to expose more of diseased tissue to lower von Mises stress than direct stenting (solid – "2 Step" or predilation included – versus respective hatched columns – "1 Step" or direct stenting – a in Figure 3), i.e. excluding predilation from the analysis (i.e. direct stenting) results in a greater volume of diseased tissue at higher von Mises stress.== The impact of pre-dilation and direct stenting on distribution of von Mises stress in atherosclerotic tissue approaches was also dependent upon the form of atherosclerosis (OgN1 and OgN6, with Mullins effect, and P2 with plasticity, Figure 3). While the OgN1 tissue representation, soft in compression and tension, is predicted to experience lower stresses overall, the P2 tissue representation, stiff in compression and tension, is predicted to experience higher stresses. The "hybrid" OgN6 representation, stiff in tension and soft in compression, is predicted to experience the highest levels of von Mises stresses. In short, inclusion of predilation technique (with a pseudo-damage constitutive tissue representation) results in slightly lower stresses than direct stenting, for all lesion types considered.

Deformed Lumen Measurements

At the end of the first phase of loading all constitutive representations predicted the same lumen configuration, viz. full recovery of the original lumen CSA, except in the P2 model with plasticity. As expected, the plasticity imbued in this representation allows permanent deformation, while the other representations are fully elastic or pseudo-elastic (Mullins effect) and recover fully on complete unloading of the tube.

The resultant deformed lumen, at maximum stent inflation and at final balloon deflation, was highly dependent on choice of base elasticity model for the diseased atherosclerotic tissue (Figure 4). As the base atherosclerotic tissue constitutive model becomes stiffer (changing from OgN1 to OgN6 to P2) the local deformations becomes smoother, i.e. the "sawtooth" effect lessens. The inclusion of stiff dispersed calcifications introduces local stiffening to the surrounding softer base atherosclerotic tissue and the contrasting change in stiffness results in the reappearance of the "sawtooth" effect (comparing top versus bottom row in Figure 4).

The inclusion of the pseudo-elastic (Mullins effect) damage model appears to have negligible effect on the soft OgN1 simulated tissue and a minor effect on the stiffer OgN6 simulated tissue. However, there is significant difference in the inclusion of plasticity to the P2 simulated tissue deformation.

Overall it can be seen in Figure 4 that each lumen profile at 2nd Inflation timepoint differs slightly when pseudo-damage is included in the atherosclerotic tissue bulk indicating again the influence predilation is having when pseudo-damage is present.

Tissue Damage Risk

More insight can be gained into the effects of the plaque constitutive representation when one examines the arterial stress state, as quantified by the predicted intimal tissue damage risk, for all variations of lesion tissue considered (Figure 5).

Post final balloon deflation, the tube is no longer applying load and predicted intimal damage is reduced as compared to maximum balloon inflation (2nd Inflation versus 2nd Deflation

in Figure 5). As the base atherosclerotic tissue constitutive model becomes stiffer (changing from OgN1 to OgN6 to P2) the predicted intimal tissue damage risk increases. Discrete calcified particles when present in the lesion induce a stiffening effect, and the predicted intimal tissue damage risk increases further, except in the stiffest lesion type (P2) where the influence of local stiffer particles is less. Interestingly, the inclusion of the Mullins type damage slightly increases predicted intimal tissue damage risk whereas the inclusion of plasticity type damage reduces predicted intimal tissue damage risk.

Atherosclerotic Tissue Stress

There is then not only an effect of specific tissue elements, atheromatous vs. sclerotic, but the relative balance between the two (Figure 6). The inclusion of a small proportion of calcifications results in an increased maximum principal stress in the atherosclerotic lesion tissue. There is minimal effect on the stress distribution by considering the Mullins effect. However the inclusion of plasticity in the P2 simulated tissue has a great effect. This is to be expected as the plasticity formulation limits the stress to 0.4 MPa (Figure 2).

Discussion

We examine the mechanical response of atherosclerotic arterial tissue to predilation followed by stent deployment and in particular the effects of the representation of plaque tissue damage using pseudo-elastic Mullins effect model, and a plasticity model. The atherosclerotic plaque tissue was itself considered as homogeneous or heterogeneous with dispersed calcified particles.

Our simulations predict that predilation induces lower maximum principal stresses in atherosclerotic tissue after overall stenting; implying that direct stenting simulations may predict higher stresses within the diseased tissue than are representative (Figure 3). This is true for all populations of diseased tissue modelled.

Implementation of the Mullins effect with the OgN1 and OgN6 plaque models has an almost negligible effect (luminal deformation curves overlapping – Figure 4) on overall deformation, consistent with *in silico* predictions for single-step stent deployment [5], but inclusion of plasticity on the P2 plaque model has a significant effect (maximum difference in deformations ~11%). The inherent softness and hence low load-carrying capacity of the OgN1 plaque material relative to arterial wall clearly shows stent strut indentations in the plaque tissue (see "sawtooth" behaviour in Figure 4(A)) and this effect is further exasperated by the presence of dispersed calcified particles for all constitutive representations. This adds insight into vascular tissue prolapse for varying different lesion types post stenting; it can be expected to have greater tissue prolapse for soft lipidic tissues (OgN1) and less tissue prolapse for stiff calcific tissue formations (P2).

Plaque material does experience damage during loading when the Mullins effect is included. Damage generated during predilation with the Mullins effect included is clear from the differences in intimal tissue damage risk at 2nd Inflation (Figure 5), where the presence of damage generated during the first loading phase results in a different stress-strain path (a softer, lower stress path). As the atherosclerotic plaque tissue model "stiffens" (progressing from OgN1 to OgN6 to P2), the predicted intimal tissue damage risk increases (Figure 5).

The inclusion of dispersed calcified particles in the plaque tissue has a further stiffening effect on the softer lesion types (OgN1 and OgN6, solid versus respective hatched columns in Figure 5), also resulting in increased predicted intimal tissue damage risk. However, the inclusion of dispersed calcified particles in a stiff diseased extracellular matrix (P2) appears to reduce predicted intimal tissue damage risk (Figure 5, solid versus respective hatched, light and dark, green columns). This can be explained by the higher positive (tensile) hoop stresses in the diseased tissue when calcifications are present (Figure 6) and also there is less luminal deformation in the presence of calcifications in a stiff diseased extracellular matrix (Figure 4-C vs 4-F). This implies that a stiff diseased extracellular matrix with embedded discrete calcifications actually has a protective effect to an underlying simulated intimal layer.

Finally, of interest is how the stress within the diseased atherosclerotic tissue is distributed, for all constitutive representations considered. It can be observed that a small proportion of calcified particles (representing 0.5% of total atherosclerotic tissue volume [5]) results in a significant increase in maximum principal stress for all constitutive representations or disease populations (see Figure 6). The highest stresses are observed in the P2 lesions models but this is

potentially not physiological as at the supra-physiological (forces beyond normal physiological loads, as applied by stenting) realm the stresses predicted could not be supported. Far more likely is the stresses predicted by the P2 model with plasticity included, as it is evident in the experimental literature that permanent deformation is possible with this tissue type. See for example, Maher *et al.* [17], where in an extensive cyclic compressive loading study, significant permanent strains on unloading for a range of plaque types were reported.

Overall, given that the clinical situation of interest is when a stent is being deployed, it can be concluded that the predilation damage of the plaque tissue, as represented here by the Mullins effect and plasticity, generates stress softening in the plaque tissue in comparison to *in silico* direct stenting approaches. As predilation is typically performed for calcified lesions the results are even more interesting in terms of luminal deformations which are highly affected by a small amount of discrete calcific particles. As we strive towards the precise quantification of vascular state post-stenting to understand complex stresses and damage caused, modelling of predilation is ever more necessary as indicated in this study, direct stenting may over estimate vascular stress distribution.

Finally, there are implications for the requirements in the stress-strain analysis section of the current FDA guideline document on non-clinical engineering tests for coronary stents in relation to finite element modelling of the physiological environment [28], on the importance of the simulation of a predilation step as part of the angioplasty technique and how this step effects plaque mechanics and stress state.

Conclusions

Idealised population models can provide insight into clinical scenarios. As shown in this study, direct stenting simulations versus those including predilation prior to stenting may over estimate vascular stress distribution. A tissue model capable of permanent deformation, in the presence of predilation, has impact on the final patient luminal area and tissue damage. A small amount of discrete micro-calcifications can be expected to increase vascular damage. As patient-specific models become more attainable, it is critical to be aware of this during procedural planning.

Acknowledgements

References

1   Kay P, Sabate M, Costa MA (eds): Cardiac Catheterization and Percutaenous Interventions. ed 1 Informa Healthcare, 2004.

2   Rogers C, Edelman ER: Endovascular Stent Design Dictates Experimental Restenosis and Thrombosis. Circulation 1995 Jun 15;91:2995–3001.

3   Edelman ER, Rogers C: Pathobiologic responses to stenting. Am J Cardiol 1998;81:4E–6E.

4   Conway C, Sharif F, McGarry J, McHugh P: A Computational Test-Bed to Assess Coronary Stent Implantation Mechanics Using a Population-Specific Approach. Cardiovasc Eng Technol 2012;3:1–14.

5   Conway C, McGarry JP, McHugh PE: Modelling of Atherosclerotic Plaque for Use in a Computational Test-Bed for Stent Angioplasty. Ann Biomed Eng 2014 Sep 11;42:2425–2439.

6   Mortier P, Holzapfel GA, De Beule M, Van Loo D, Taeymans Y, Segers P, et al.: A novel simulation strategy for stent insertion and deployment in curved coronary bifurcations: Comparison of three drug-eluting stents. Ann Biomed Eng 2010;38:88–99.

7   Zahedmanesh H, John Kelly D, Lally C: Simulation of a balloon expandable stent in a realistic coronary artery--Determination of the optimum modelling strategy. J Biomech 2010;43:2126–2132.

8   Gastaldi D, Morlacchi S, Nichetti R, Capelli C, Dubini G, Petrini L, et al.: Modelling of the provisional side-branch stenting approach for the treatment of atherosclerotic coronary bifurcations: effects of stent positioning. Biomech Model Mechanobiol 2010;9:551–561.

9   Gijsen F, Migliavacca F, Schievano S, Socci L, Petrini L, Thury A, et al.: Simulation of stent deployment in a realistic human coronary artery. Biomed Eng OnLine 2008;7. DOI: 10.1186/1475-925X-7-23

10   Morlacchi S, Migliavacca F: Modeling stented coronary arteries: where we are, where to go. Ann Biomed Eng 2013 Jul;41:1428–44.

11   Martin D, Boyle FJ: Computational structural modelling of coronary stnet deployment: a review. Comput Methods Biomech Biomed Engin 2011;14:331–348.

12   Zahedmanesh H, Lally C: Determination of the influence of stent strut thickness using the finite element method: implications for vascular injury and in-stent restenosis. Med Biol Eng Comput 2009;47:385–393.

13 Zahedmanesh H, John Kelly D, Lally C: Simulation of a balloon expandable stent in a realistic coronary artery--Determination of the optimum modelling strategy. J Biomech 2010;43:2126–2132.

14 O'Reilly BL, Conway C, McGarry JP, McHugh PE: Arterial and Atherosclerotic Plaque Biomechanics with Application to Stent Angioplasty Modeling; in Holzapfel GA, Ogden RW (eds): Biomechanics: Trends in Modeling and Simulation. Springer International Publishing, 2017, pp 193–231.

15 Ogden RW, Roxburgh DG: A pseudo-elastic model for the Mullins effect in filled rubber. Proc R Soc Lond A 1999;455:2861–2877.

16 Miehe C: Discontinuous and continuous damage evolution in Ogden type large stgrain elastic materials. Eur J Mech ASolids 1995;14:697–720.

17 Maher E, Creane A, Sultan S, Hynes N, Lally C, Kelly DJ: Inelasticity of Human Carotid Atherosclerotic Plaque. Ann Biomed Eng 2011 May;39:2445–2455.

18 Peña E, Doblaré M: An anisotropic pseudo-elastic approach for modelling Mullins effect in fibrous biological materials. Mech Res Commun 2009;36:784–790.

19 Balzani D, Schröder J, Gross D: Simulation of discontinuous damage incorporating residual stresses in circumferentially overstretched atherosclerotic arteries. Acta Biomater 2006 Nov;2:609–618.

20 Peña E, Peña JA, Doblaré M: On the Mullins effect and hysteresis of fibered biological materials: A comparison between continuous and discontinuous damage models. Int J Solids Struct 2009 Apr;46:1727–1735.

21 Calvo B, Peña E, Martinez MA, Doblaré M: An uncoupled directional damage model for fibred biological soft tissues. Formulation and computational aspects. Int J Numer Methods Eng 2007;69:2036–2057.

22 Dassault Systemes: Abaqus 6.13 Documentation. 2013.

23 Stary H: Atlas of Atherosclerosis Progression and Regression. New York/London, Parthenon Publishing, 1999.

24 Grogan JA, Leen SB, McHugh PE: Comparing coronary stent material performance on a common geometric platform through simulated bench testing. J Mech Behav Biomed Mater 2012 Aug;12:129–38.

25 Loree HM, Grodzinsky AJ, Park SY, Gibson LJ, Lee RT: Static circumferential tangential modulus of human atherosclerotic tissue. J Biomech 1994;27:195–204.

26 Ebenstein DM, Coughlin D, Chapman J, Li C, Pruitt LA: Nanomechanical properties of calcification, fibrous tissue, and hematoma from atherosclerotic plaques. J Biomed Mater Res A 2009 Dec;91A:1028–1037.

27 Holzapfel GA, Sommer G, Regitnig P: Anisotropic mechanical properties of tissue components in human atherosclerotic plaques. J Biomech Eng 2004;126:657–665.

28 FDA: Non-Clinical Engineering Tests and Recommended Labeling for Intravascular Stents and Associated Delivery Systems. Guid Ind FDA Staff 2010 [cited 2014 Apr 22];1–51.
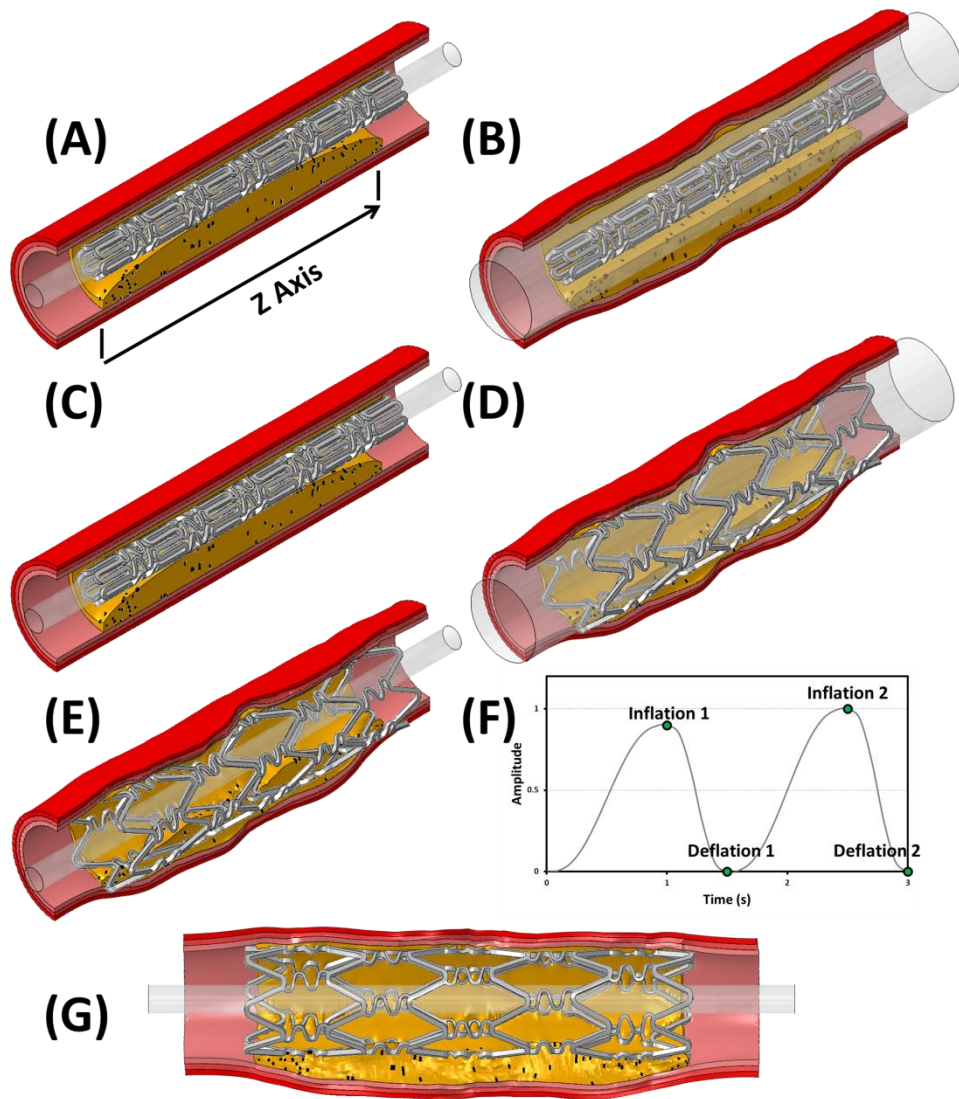
Figure 1: Model of stenotic artery used in the simulations showing stages of stent deployment with a stiff elastic tube. (A) Pre-deployment, (B) Maximum 1st Inflation, with contact between the stent and tube turned off, (C) Post tube 1st Deflation, (D) Maximum 2nd Inflation, with contact between stent and tube turned on, and (E) Post tube 2nd Deflation. (F) Amplitude loading curve for two-phase stiff tube expansion simulations, with the amplitude of 1st Inflation being 90% of 2nd Inflation and (G) Long-axis view of deformed configuration with discrete micro-calcifications shown in black.
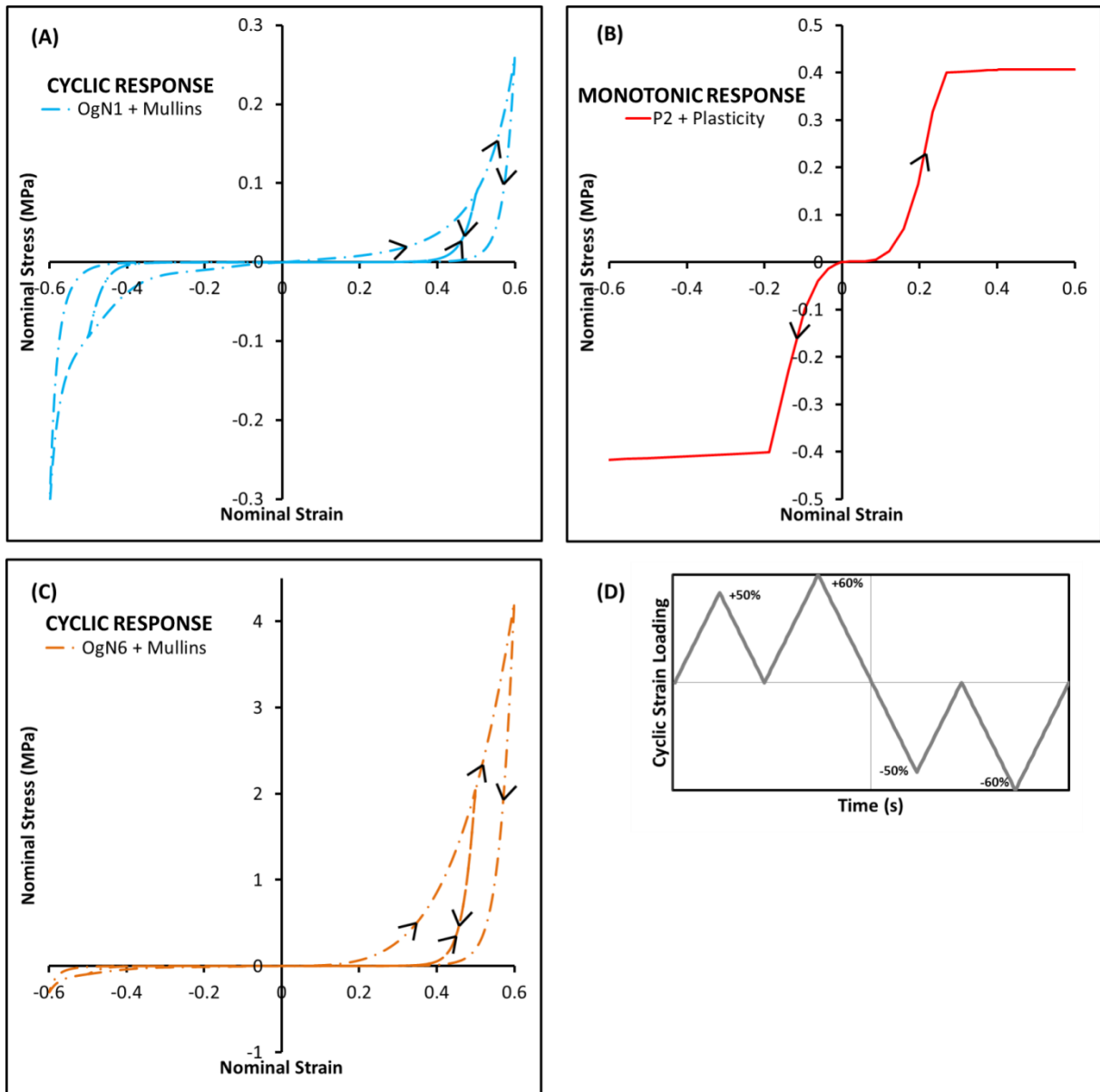
Figure 2   Response of different constitutive models to cyclic and monotonic loading in tension and compression illustrated. (A) Cyclic response of the first order Ogden (OgN1) model, with Mullins effect, (B) Monotonic response of second order polynomial model (P2) with plasticity, (C) Cyclic response of the sixth order Ogden (OgN6) model, with Mullins effect, and (D) Cyclic strain loading amplitude used to generate the response shown in (A) & (C).
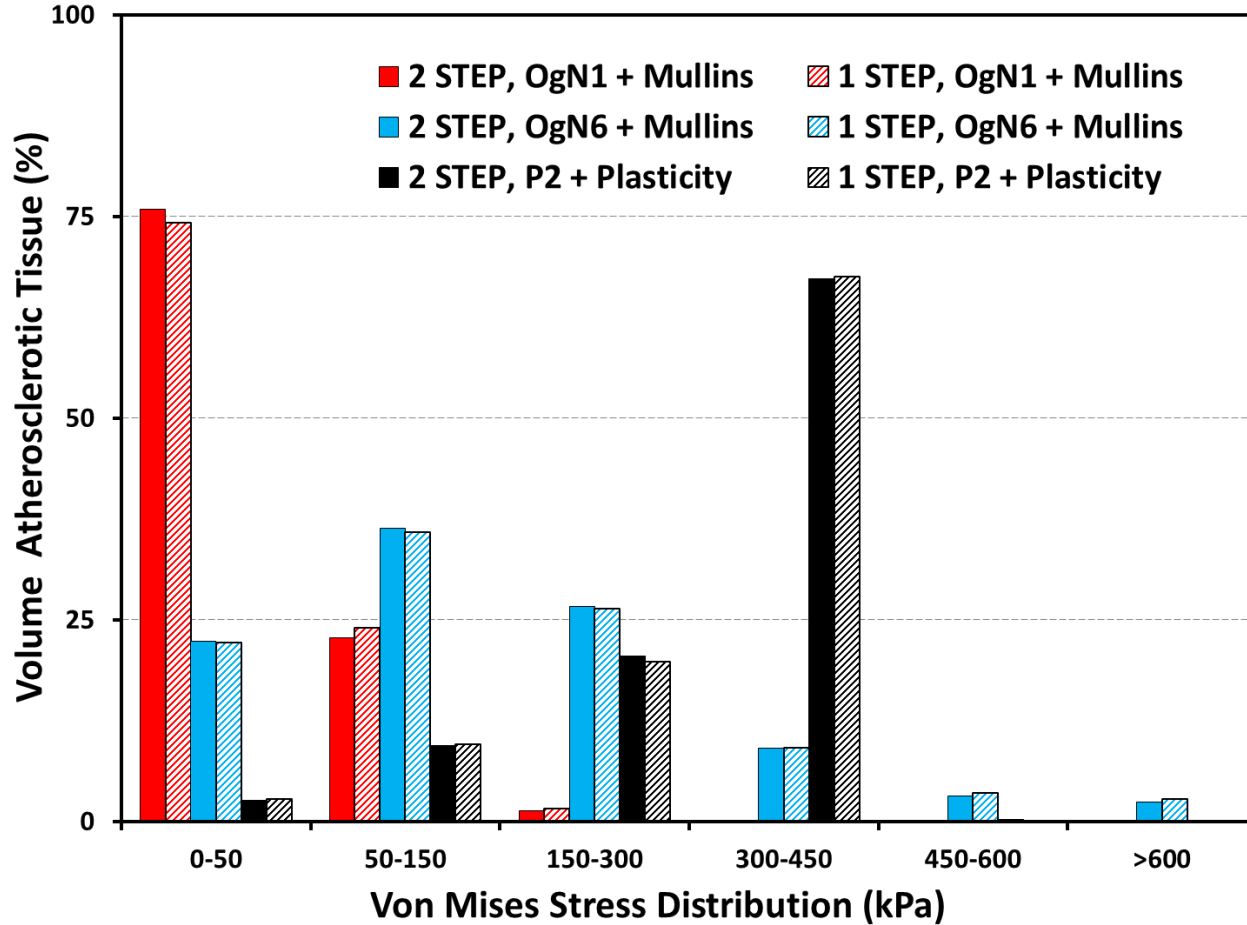
Figure 3   Von Mises stress distribution for percent volume of atherosclerotic tissue in pre-dilation (2 STEP) and direct stenting (1 STEP) simulations, at maximum stent inflation, for three damage model representations: first order Ogden (OgN1) with Mullins effect, sixth order Ogden (OgN6) with Mullins effect and second order polynomial (P2) with plasticity.
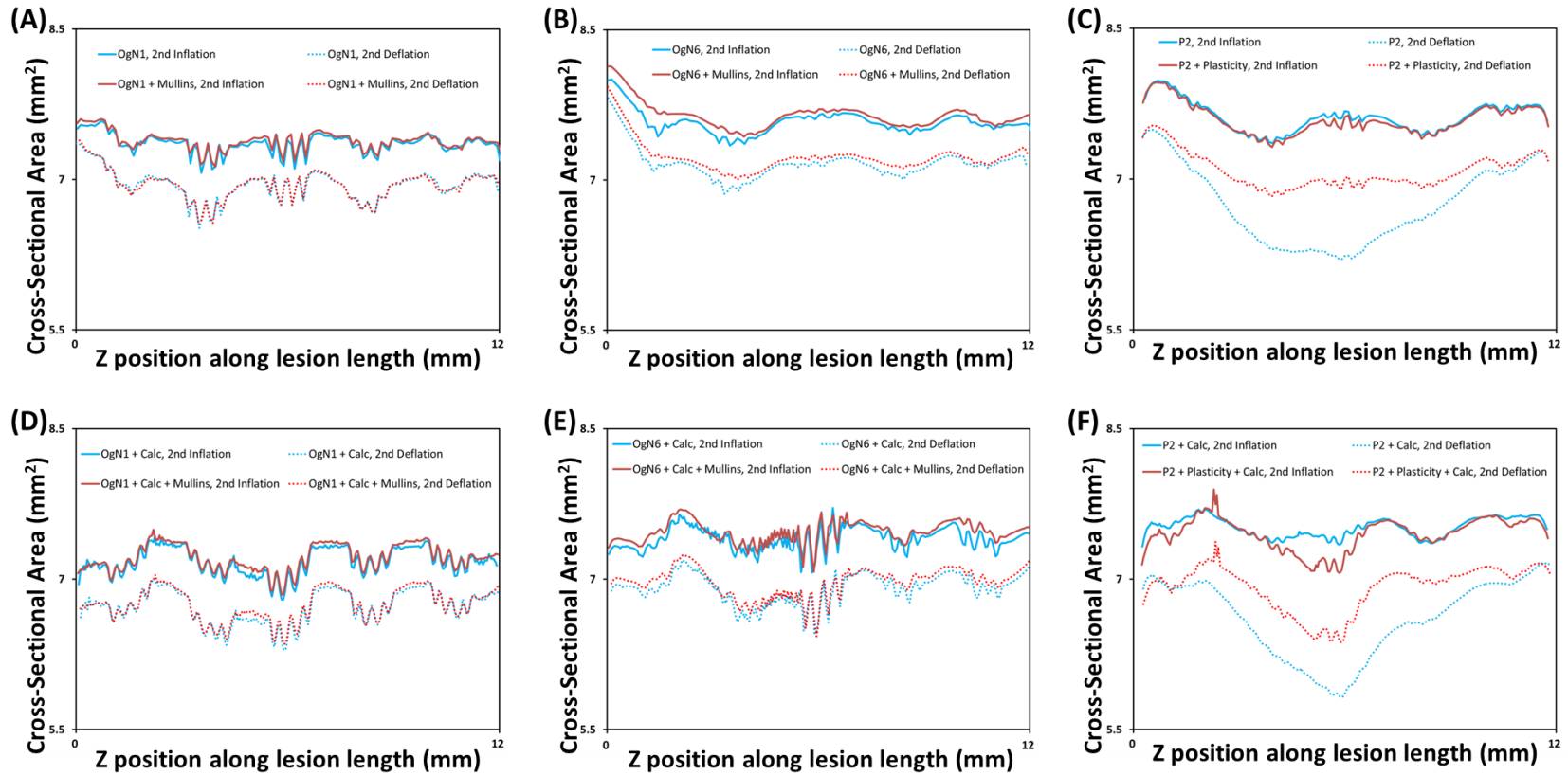
Figure 4 Cross-sectional area measurements along the length of the atherosclerotic tissue geometry, Z position along lesion length (see Figure 1(A)), for six different constitutive representations: (A) first order Ogden (OgN1), with and without Mullins effect, (B) sixth order Ogden (OgN6), with and without Mullins effect, (C) second order polynomial (P2), with and without plasticity, (D) first order Ogden (OgN1), with and without Mullins effect, with discrete calcifications (E) sixth order Ogden (OgN6), with and without Mullins effect, with discrete calcifications and (F) second order polynomial (P2), with and without plasticity, with discrete calcifications. Two time points in the second phase of the two-phase expansion simulations shown: 2nd Inflation and 2nd Deflation (please refer to Figure 1(F)).
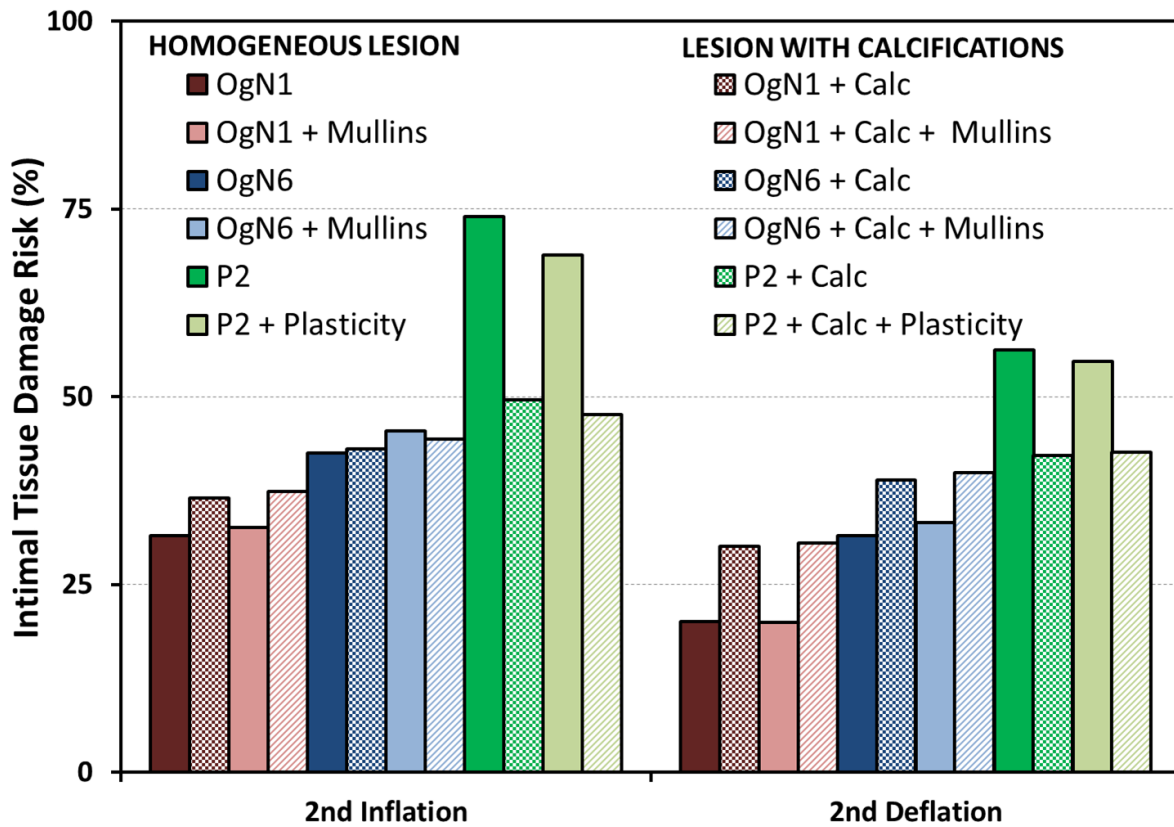
Figure 5   Predicted percent tissue damage risk in the intimal layer results for two-phase expansion simulations, at two time points: 2nd Inflation and 2nd Deflation, (refer to Figure 1). Simulations included both homogenous lesions and lesions with diffuse discrete calcifications for six different constitutive representations: first order Ogden (OgN1), with and without Mullins effect, sixth order Ogden (OgN6), with and without Mullins effect and second order polynomial (P2), with and without plasticity.
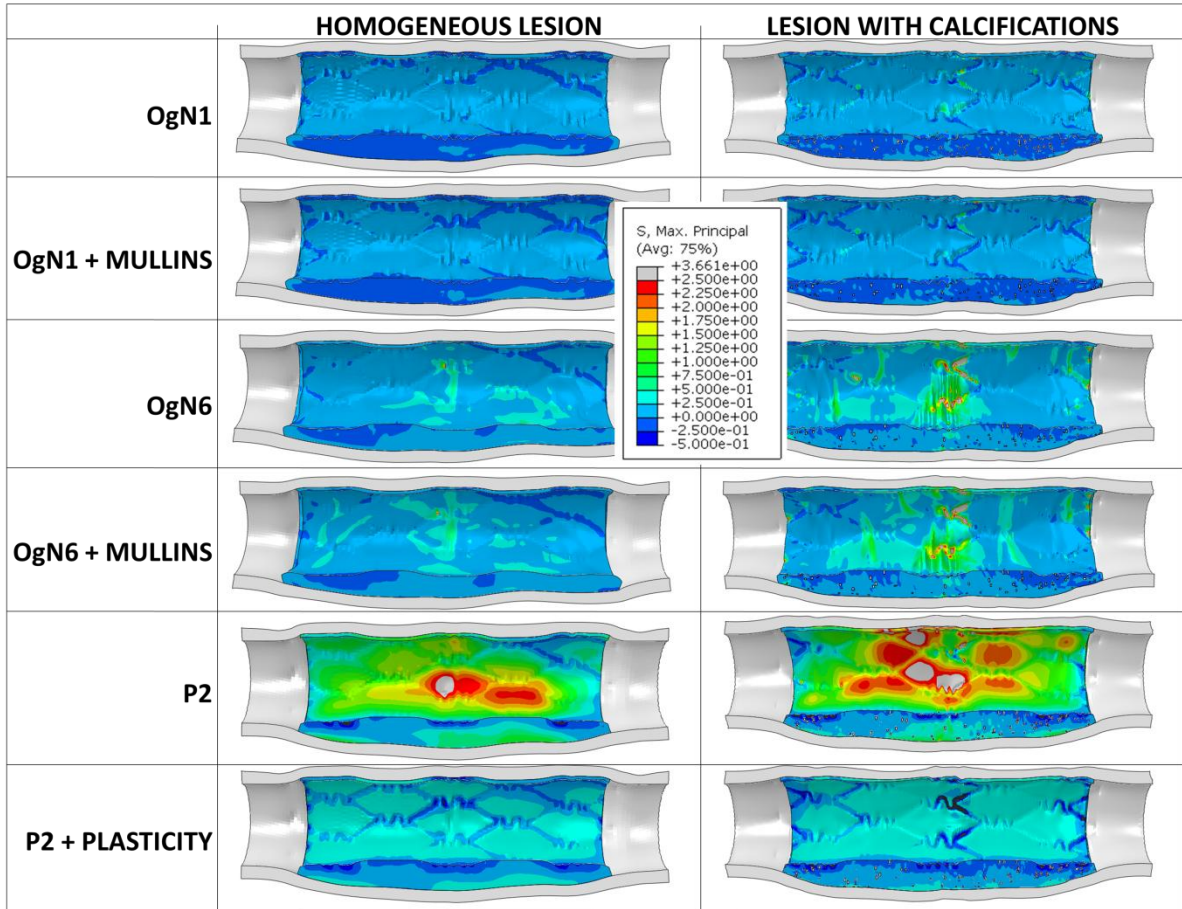
Figure 6   Maximum Principal Stress distribution (MPa) in atherosclerotic tissue, both homogenous and with diffuse discrete calcifications (in white) for six different constitutive representations: first order Ogden (OgN1), with and without Mullins effect, sixth order Ogden (OgN6), with and without Mullins effect and second order polynomial (P2), with and without plasticity. All distributions are shown at second inflation timepoint (please refer to Figure 1(F)).